Rare Metal Materials and Engineering
Volume 48, Issue 6, June 2019
Available online at www.rmme.ac.cn

Science Press

Cite this article as: Rare Metal Materials and Engineering, 2019, 48(6): 1769-1776.

ARTICLE

Thermodynamic Analysis and Experimental Investigation of Mg-9Zn-*X*Al Alloy for Semi-Solid Forming

Li Chun[1,2], Cui Le[1], Fan Xinhui[1,2], Chen Jian[1,2], Li Ying[1], Yuan Xunfeng[1], Li Yuandong[3]

[1] Shaanxi Key Laboratory of Comprehensive Utilization of Tailings Resources, Shangluo University, Shangluo 726000, China; [2] Xi'an Technological University, Xi'an 710021, China; [3] State Key Laboratory of Advanced Processing and Recycling of Non-ferrous Metals, Lanzhou University of Technology, Lanzhou 730050, China

Abstract: Solidification temperature range, temperature sensitivity of the solid fraction, temperature process window and phase composition and transformation path of Mg-9Zn-*X*Al (*X*=2, 4, 6, wt%) alloys were calculated by Pandat calculation, and studied by experiment. The results indicate that a larger temperature window is conducive to the control and operation of semi-solid forming for the Mg-9Zn-*X*Al alloy. The temperature sensitivity of all solid fractions is smaller than 0.015. Mg-9Zn-*X*Al alloys have different transformation temperatures and paths of the phase at different Al additions. α-Mg, MgZn, $Mg_{32}(Al, Zn)_{49}$ and $Al_5Mg_{11}Zn_4$ are formed in all samples. When Al addition is increased to 6%, $Mg_{17}Al_{12}$ phase is formed. The grain size and roundness of Mg-9Zn-*X*Al alloys prepared by self-inoculation rheo-diecasting method are 65.3, 56.5, 52.2 μm and 1.3, 1.19, 1.23, respectively. When the working temperature is 150 °C, the comprehensive strength and deformation are 278, 283, 295 MPa and 36.22%, 33.02%, 31.21%, respectively.

Key words: thermodynamic calculation; Mg-9Zn-*X*Al; semi-solid forming; phase transformation

In recent years, lightweight materials in the fields such as automobile and aerospace etc have been required, which lead to an increase in the dosage of aluminum and magnesium alloys in these fields[1]. Compared with aluminum alloys, magnesium alloys are lighter, but Mg alloys exhibit poor resistance and poor mechanical properties. Magnesium alloys which are prepared by traditional casting have a lot of defects. After Flemings developed semi-solid forming, many scholars have used this technology and formed high quality castings, which have good compactness, lower porosity, and can be strengthened by heat treatment[2,3]. However, many scholars have committed themselves to studying the microstructure and properties by adding elements, changing Zn/Al ratios, and heat treatment[4-6]. There are very few studies on high Zn magnesium alloys that were formed by semi-solid metal (SSM) casting. Selected alloy types can be developed with semi-solid forming through thermodynamic calculation for alloys. Information can be provided by thermodynamic analysis for semisolid processing of an alloy[7].

Agnew et al[8] pointed out that thermodynamic modeling is useful for computational materials science and engineering approaches in alloy development. The process temperature, sensitivity, freezing ranges, and the detailed constitution are essential for semi-solid forming of an alloy. These parameters are obtained by thermodynamic calculation. To choose and design better semi-solid alloys, metal solidification and the quantity of the precipitated phase are calculated by combining computer software with a thermodynamic database. Atkinson et al[9] predicted the 7000 series Al-Zn-Mg-Cu system alloy composition, amenable to semi-solid processing, using thermodynamic calculation. Liu[10] et al studied the effect of added copper on the thixoformability of alloy A356 and the

Received date: June 20, 2018
Foundation item: National Natural Science Foundation of China (51464031, 51471123); Scientific Research Plan of Shaanxi Education Department (16JK1241); Planned Science and Technology of Shangluo City (SK2016-29)
Corresponding author: Fan Xinhui, Ph. D., Professor, School of Materials and Chemical Engineering, Xi'an Technological University, Xi'an 710021, P. R. China, E-mail: fxh_slxy@163.com

effect of added silicon on the thixoformability of alloy 2014, which used MTDATA and thermodynamic and phase equilibrium software combined with the MTAL database. Li et al[11] studied alloy optimization with thermodynamic simulations for semisolid processing of commercial AM60 alloy. The effects of various alloying elements on the solidification behavior and SSM processability of AM60 alloy were calculated by Pandat software. GrÖbner et al[12] investigated phase equilibria and transformation in ternary Mg-Cd-Zn alloys. Liu[13] predicted the major phases of a high zinc-containing Al-Zn-Mg-Cu alloy in an experiment with thermodynamic calculation. Xia et al[14] studied ternary phases in an Mg-Zn-Sm system at the Mg-rich corner by thermodynamic modeling and experimental investigation. However, there was a small amount of high Znic magnesium alloy, which was calculated by thermodynamic analysis for semisolid processing.

In this work, Mg-9Zn-*X*Al(*X*=2, 4, 6, wt%) alloys, used for semisolid processing, were optimized by thermodynamic calculation. The feasibility of Mg-9Zn-*X*Al alloys for semi-solid forming was analyzed, and they were validated by experiment. Meanwhile, the effects of Al content on forming feasibility and microstructure and phases were investigated.

1 Calculation Model and Experiment

1.1 Materials

To study the semisolid processability of Mg-9Zn-*X*Al alloy, their chemical components are given in Table 1. All calculations and experiments were based on these composition to analyze the semisolid processability of Mg-9Zn-*X*Al alloys.

1.2 Calculation model

Pandat software (Computherm, Madison, WI. USA) was used to calculate the solidification process of Mg-9Zn-*X*Al alloy, which includes solidification temperature range, temperature sensitivity of the solid fraction, temperature process window, and phase transformation. The solidification model was chosen as non-equilibrium (Scheil). The calculation of the solidification process was carried out by inputting the various alloying elements (Mg, Zn and Al) at different levels and allowing Pandat software to calculate the solidification process for their respective mass fractions in the alloy at selected temperatures. The Pandat database PanMg8 was used in the calculations[15].

1.3 Experiment

In this study, semi-solid billets were prepared by self-inoculation method (SIM), and the process route is illustrated in Fig.1. The alloys used in this study were novel high Zn magnesium alloys, which include ZA92, ZA94 and ZA96.

Table 1 Chemical components of experimental alloy (wt%)

Alloy	Zn	Al	Mg
ZA92	9	2	Bal.
ZA94	9	4	Bal.
ZA96	9	6	Bal.

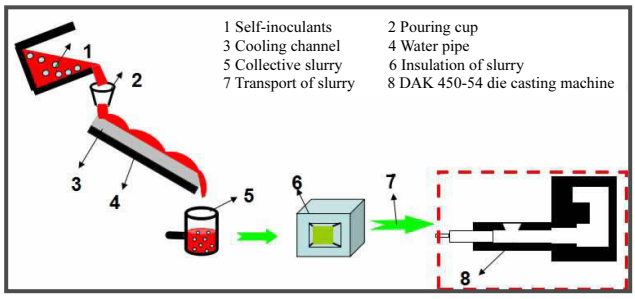

Fig.1 Schematic of self-inoculation rheo-diecasting

Commercially pure Mg, Zn, and Al were used in an SG2-75-10 resistance furnace with a steel crucible of 108 mm in diameter and 250 mm in height. The whole process was conducted under the cover of a protective atmosphere (Ar). A K-type thermo-couple was inserted into the middle of the crucible to measure the temperature of the melt. The Mg-9Zn-*X*Al alloy was melted and held at 700 °C for 10 min, and degassed by C_2Cl_6 at 730 °C. The melted Mg-9Zn-*X*Al magnesium alloy was treated by SIM under the same super heat of 80 °C. Then, the billets were formed by a die casting machine.

The samples were etched with an etchant 4 vol% nital. Differential scanning calorimetry (DSC) was performed using a NETZSCH STA 409C/CD instrument. The test was performed at a heating rate of 10 °C/min from room temperature up to 650 °C. The microstructures and phases were analyzed by OM and XRD.

2 Thermodynamic Analysis of Mg-9Zn-*X*Al Alloy

An alloy for semi-solid processing should meet three criteria for the controllability of the forming process[16]: (1) The solidification range of an semi-solid method (SSM) alloy should be from 20 °C to 130 °C. (2) In a range of the solid fraction that is suitable for semi-solid forming, the temperature sensitivity of solid fraction, which is -d*f*s/d*T*, should be less than 0.015. (3) The temperature process window should be more than 6 °C.

2.1 Solidification temperature range

The solidification temperature range is usually defined as the temperature range between the solidus and the liquidus of an alloy. The solidification temperature range is zero for pure metal and eutectic alloy. However, the alloy has a wide solidification temperature range, and the wider solidification is conducive to semi-solid forming. Alloys with a too wide solidification temperature range may be subjected to hot tearing. Hence, the solidification range of an SSM alloy should be from 20 °C to 130 °C.

The solid fraction vs temperature curves of Mg-9Zn-*X*Al, solidified under non-equilibrium conditions, were calculated by Pandat software. From the result of calculations, as shown

in Fig.2 and Table 2, with Al contents increasing, the liquidus temperature decreases, and the solidus temperature basically remains unchanged. So, the solidification temperature range (ΔT=$T(\varphi_s$=0)–$T(\varphi_s$=1)) of Mg-9Zn-*X*Al decreases. When Al additions are 2%, 4%, and 6%, the solidification temperatures range are 271.5, 259.5, and 247.3 °C, respectively.

In the forming process, the solidification temperature range of semi-solid forming is not ΔT, and the available temperature range of SSM processing is smaller than that from liquidus to solidus. Hence, for SSM processing, an available solidification temperature range (ΔT_{ATR}) should be the range of temperature from a suitable SSM processing temperature to the eutectic temperature. The secondary solidification phase, with hot tearing and pores of the alloy, are affected by ΔT_{ATR}. SSM processing includes rheo-forming and thixo-forming, and the rheo-forming ΔT_{ATR} and thixo-forming ΔT_{ATR} are different for the same alloy. The rheo-forming ΔT_{ATR} is defined as $T(\varphi_s$=0.4)–$T(\varphi_s$=1), and the thixo-forming ΔT_{ATR} is defined as $T(\varphi_s$=0.6)–$T(\varphi_s$=1). From the result of calculations as shown in Table 2, with Al addition increasing, ΔT_{ATR} decreases. When Al addition is 2%, 4%, and 6%, the rheo-forming ΔT_{ATR} is 236.3, 202.6 and 185.2 °C, respectively, and the thixo-forming ΔT_{ATR} is 207.5, 166.9, and 139.9 °C.

The calculation data were compared with the experimental results using DCS with a heating rate of 5 °C/min. Gottardi et al[17] showed that DSC is an optimal tool for measuring the actual solid fraction of an alloy. DSC curves of Mg-9Zn-*X*Al are given in Fig.3. The DSC curves have two large peaks, which represent the eutectic and the liquidus temperatures. It can be seen that Al addition has a significant impact on the solidification process. With Al addition increasing, the DSC curves of the experimental alloys have an obvious change. The peak value of the eutectic temperature is moved right, and the peak value of the nucleation temperature is moved left. The

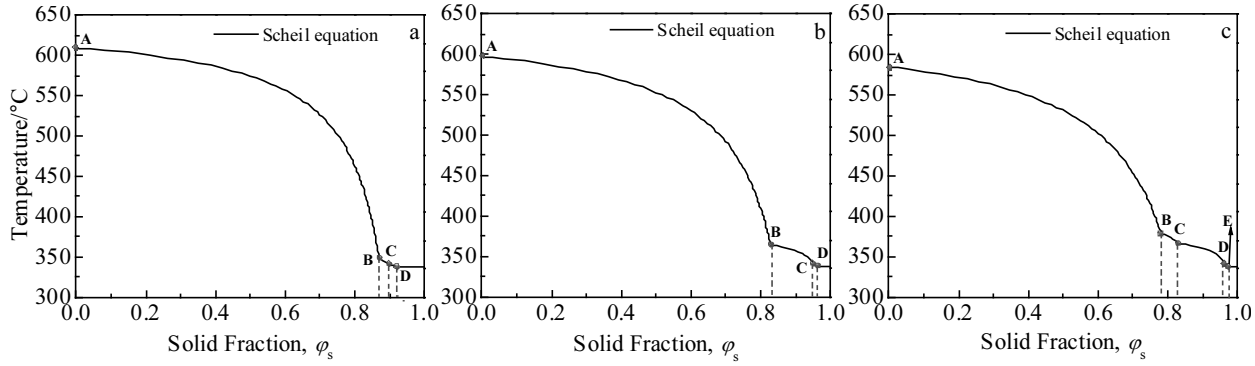

Fig.2 Temperature vs solid fraction curves for Mg-9Zn-*X*Al alloy: (a) ZA92, (b) ZA94, and (c) ZA96

Table 2 Solidification temperature ranges of Mg-9Zn-*X*Al alloys (°C)

Alloy	φ_s=0	φ_s=0.4	φ_s=0.6	φ_s=1	Rheo-forming, ΔT_{ATR}	Thixo-forming, ΔT_{ATR}
ZA92	609.6	584.0	555.2	338.1	236.3	207.5
ZA94	597.6	566.2	530.5	338.1	202.6	166.9
ZA96	585.4	548.8	503.5	338.1	185.2	139.9

eutectic temperature is 337.2, 346.7, and 351.6 °C, and the nucleation temperature is 614.7, 590.2, and 582.1 °C, respectively, for ZA92, ZA94 and ZA96 alloy. The experimental results are basically the same as the calculated results by Pandat software.

2.2 Temperature sensitivity of solid fraction

The solid fraction is an important part of semi-solid forming.

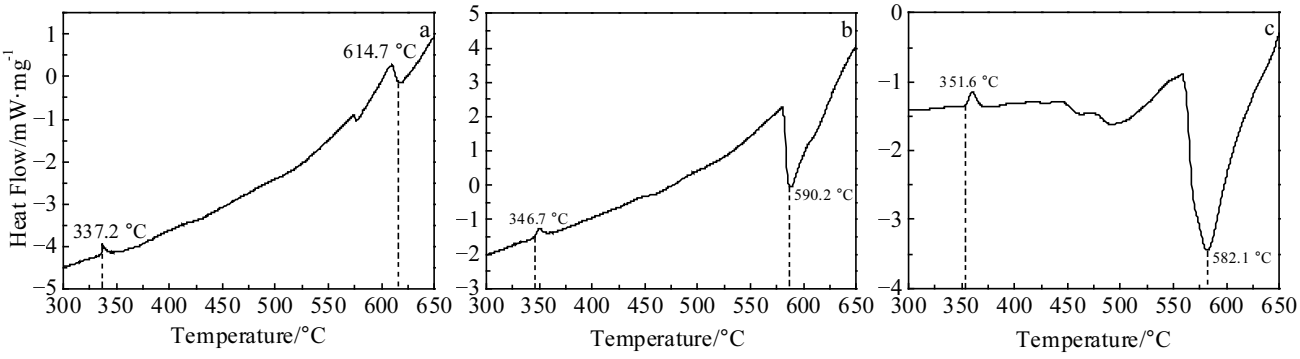

Fig.3 DSC curves of Mg-9Zn-*X*Al alloy: (a) ZA92, (b) ZA94, and (c) ZA96

Temperature sensitivity of solid fraction is defined as the negative derivative of the temperature vs solid fraction curve, i.e. $-d\varphi_s/dT$. Semi-solid processing performance of the alloy is affected greatly by the temperature sensitivity of the solid fraction. When $-d\varphi_s/dT$ is larger, the slope of the temperature vs solid fraction curve is larger. Therefore, a smaller transformation of the temperature leads to a solid fraction that causes a larger transformation. For semi-solid forming, when $-d\varphi_s/dT$ is small, the alloy melt temperature is easy to control.

Fig.4 shows the relationship between the solid fraction and temperature sensitivity of Mg-9Zn-*X*Al. With Al addition increasing, the solid fraction decreases. When $-d\varphi_s/dT$ is 0.015, the solid fraction is about 25%, 18%, and 5%, respectively, for ZA92, ZA94 and ZA96. Fig.4 shows that the solid fraction of three points (a, b, c) is 30%, 50%, and 70%, respectively, and their temperature sensitivities are less than 0.015. Hence, Mg-9Zn-*X*Al (*X*=2, 4, 6) can be used for rheo-forming as well as thixo-forming.

2.3 Temperature process window

Fig.5 shows the relationship between the temperature process window and the solid fraction. The semi-solid temperature process window is also known as the temperature processing window. For semi-solid forming, the absolute error leads to a fluctuation of processing temperature during experimental operation. Therefore, an understanding of the semi-solid processing temperature window, with an accurate grasp of the fluctuation of the melt treatment temperature during forming, is needed, to accurately control the semi-solid

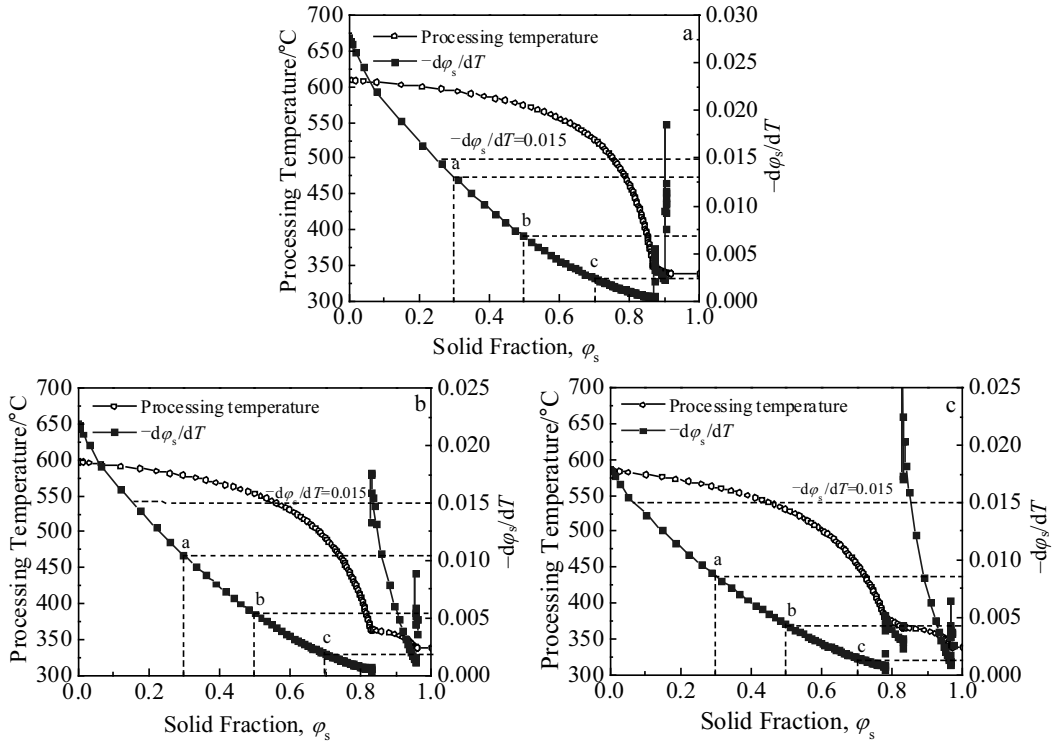

Fig.4 Relationship between solid fraction and sensitivity of temperature for Mg-9Zn-*X*Al alloy: (a) ZA92, (b) ZA94, and (c) ZA96

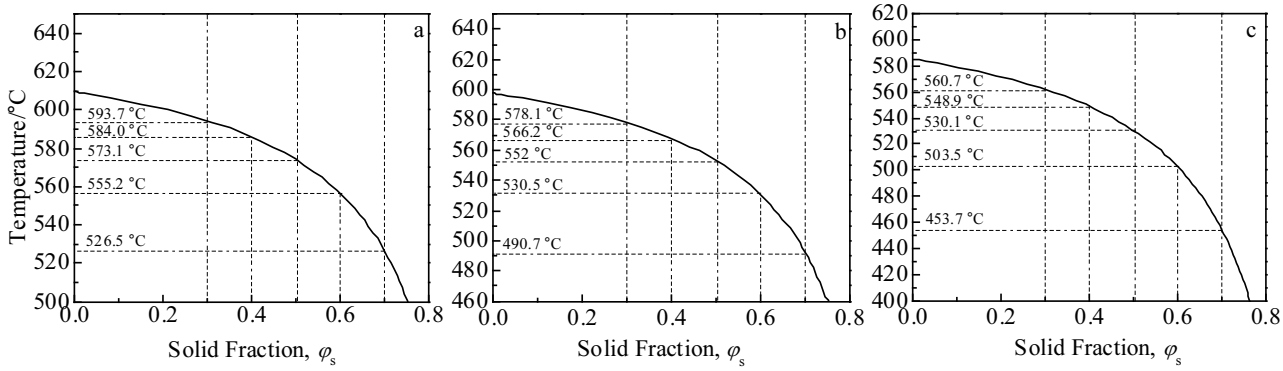

Fig.5 Relationship between temperature process window and solid fraction for Mg-9Zn-*X*Al alloy: (a) ZA92, (b) ZA94, and (c) ZA96

processing temperature. The ideal solid fraction is 0.3~0.5 and 0.5~0.7, respectively, for rheo-forming and thixo-forming. The semi-solid temperature window is the corresponding temperature range of the solid fraction.

The corresponding temperatures of different solid fractions (φ_s=0.3, 0.4, 0.5, 0.6, 0.7) are marked. The semi-solid processing temperature window ΔT_{TPW} is $T(\varphi_s=0.3)$–$T(\varphi_s=0.5)$ for rheo-forming and $T(\varphi_s=0.5)$–$T(\varphi_s=0.7)$ for thixo-forming. After calculation (as shown in Table 3), semi-solid processing temperature window of rheo-forming are 20.6, 26.1, and 30.6 °C, and semi-solid processing temperature window of the thixo-forming are 22.6, 61.3 and 76.4 °C, for ZA 92, ZA94, and ZA96, respectively. With Al addition increasing, the semi-solid processing temperature window of the Mg-9Zn-*X*Al alloy increases. The larger temperature window is conducive to the control and operation of semi-solid forming. Therefore, compared with ZA92 and ZA94, ZA96 magnesium alloy is easy for semi-solid forming.

2.4 Phase transformation

For an extremely slow cooling rate, the ideal solidification of an alloy fits the lever rule model. However, the solidification process of most alloys is nonequilibrium solidification, in practice. Hence, the solidification of the Mg-9Zn-*X*Al alloy was analyzed by the Scheil equation model. Fig.6 shows the amount of each individual phase and the temperature range over which it is formed. The detailed phases of the Mg-9Zn-*X*Al alloy, and the mass fraction of each phase were calculated. α-Mg, $Al_5Mg_{11}Zn_4$, $Mg_{32}(Al, Zn)_{49}$, and MgZn phases appear in the Mg-9Zn-*X*Al alloy, and the $Mg_{17}Al_{12}$ phase can be found in Mg-9Zn-6Al alloy. Anyanwu et al[18] found that when the sum of w(Zn) and w(Al) is 13% and the ratio of the mass of Zn to Al is 2, the Mg-(6~14)Zn-(2~8)Al magnesium alloy is composed of α-Mg, $Mg_{32}(Al, Zn)_{49}$ and MgZn phases. The transition path of phases is described by Fig.2, and the points (including A, B, C, D and E) show the phase transformation temperatures. The phase transformation and reaction of Mg-9Zn-*X*Al alloys are shown in Table 4.

Table 3 Temperature process window of Mg-9Zn-*X*Al magnesium alloy at semi-solid state (°C)

Alloy	φ_s=0.3	φ_s=0.5	φ_s=0.7	Rheo-forming, ΔT_{TPW}	Thixo-forming, ΔT_{TPW}
ZA92	593.7	573.1	526.5	20.6	22.6
ZA94	578.1	552	490.7	26.1	61.3
ZA96	560.7	530.1	453.7	30.6	76.4

From Fig.2 and Fig.6, it is shown that crystallization of Mg-9Zn-*X*Al alloys begins with the solidification of a magnesium solid solution (α-Mg), and the transition path is from point A to point B in Fig.2a~2c. With a decrease of solidification temperature, the precipitation path of $Al_5Mg_{11}Zn_4$, $Mg_{32}(Al, Zn)_{49}$, and MgZn phases are point B to point C, point C to point D and point D to the end for Mg-9Zn-*X*Al (*X*=2, 4). The precipitation path of the $Mg_{17}Al_{12}$, $Al_5Mg_{11}Zn_4$, $Mg_{32}(Al, Zn)_{49}$, and MgZn phases are point B to point C, point C to point D, point D to point E and point E to the end for Mg-9Zn-6Al. With increasing Al content, the transformation temperature of α-Mg phase decreases, but the transformation temperatures of $Mg_{32}(Al, Zn)_{49}$ and MgZn phases are the same. The detailed transformation temperatures of the phases are shown in Table 4.

XRD analysis results of Mg-9Zn-*X*Al alloys are shown in Fig.7. Fig.7 clearly reveals the phase composition at different Al additions. In all the samples, α-Mg, MgZn and $Mg_{32}(Al, Zn)_{49}$ are identified. $Al_5Mg_{11}Zn_4$ and $Mg_{17}Al_{12}$ phases are not found in the ZA92 magnesium alloy. Xing et al[19] considered that when the ratio of the mass of Zn to Al of the alloys is more than 2, the alloys are composed of α-Mg, $Mg_{32}(Al, Zn)_{49}$, and MgZn phases. The $Al_5Mg_{11}Zn_4$ phase is near 48° in ZA94 and ZA96, and the $Mg_{17}Al_{12}$ phase is near 36.3° in the ZA96 magnesium alloy.

Through the above analysis, the Mg-9Zn-*X*Al alloy can be formed by semi-solid processing. The effects of Al content on thermodynamic parameters and phase transformation were analyzed. For further analysis, Mg-9Zn-*X*Al alloy was formed by SIM. The following experiment was based on the above thermodynamic analysis.

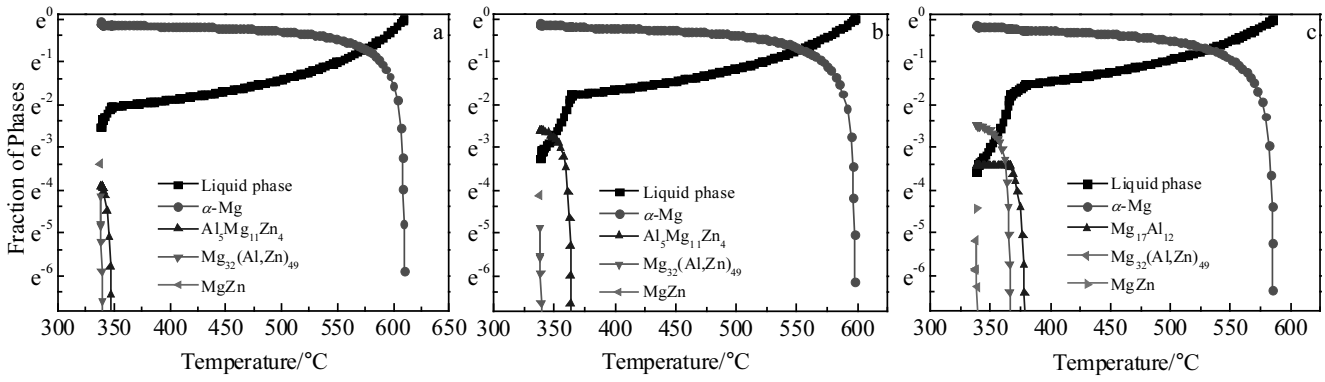

Fig.6 Calculated molar fraction of all solidified phases of Mg-9Zn-*X*Al alloy: (a) ZA92, (b) ZA94, and (c) ZA96

Table 4 Reaction of Mg-9Zn-*X*Al alloy during phase transformation

Alloy	Reaction
ZA92	$L \xrightarrow{609.6\ ^\circ C} \alpha\text{-Mg}$
	$L \xrightarrow{347.7\ ^\circ C} \alpha\text{-Mg} + Al_5Mg_{11}Zn_4$
	$L \xrightarrow{339.7\ ^\circ C} \alpha\text{-Mg} + Mg_{32}(Al,Zn)_{49}$
	$L \xrightarrow{338.1\ ^\circ C} \alpha\text{-Mg} + Mg_{32}(Al,Zn)_{49} + MgZn$
ZA94	$L \xrightarrow{597.6\ ^\circ C} \alpha\text{-Mg}$
	$L \xrightarrow{363.6\ ^\circ C} \alpha\text{-Mg} + Al_5Mg_{11}Zn_4$
	$L \xrightarrow{339.7\ ^\circ C} \alpha\text{-Mg} + Mg_{32}(Al,Zn)_{49}$
	$L \xrightarrow{338.1\ ^\circ C} \alpha\text{-Mg} + Mg_{32}(Al,Zn)_{49} + MgZn$
ZA96	$L \xrightarrow{585.4\ ^\circ C} \alpha\text{-Mg}$
	$L \xrightarrow{379\ ^\circ C} \alpha\text{-Mg} + Al_{12}Mg_{17}$
	$L \xrightarrow{366.2\ ^\circ C} \alpha\text{-Mg} + Al_5Mg_{11}Zn_4$
	$L \xrightarrow{339.7\ ^\circ C} \alpha\text{-Mg} + Mg_{32}(Al,Zn)_{49}$
	$L \xrightarrow{338.1\ ^\circ C} \alpha\text{-Mg} + Mg_{32}(Al,Zn)_{49} + MgZn$

3 Semi-solid Microstructure of Mg-9Zn-XAl Alloy Prepared by SIM

Fig.8 shows the microstructures of the Mg-9Zn-*X*Al alloy prepared by the self-inoculation process under the best technology conditions. The white phase is primary α-Mg and secondary solidified microstructure (smaller white parts), and the dark continuous matrix is the eutectic phase, which is similar to the result reported by Xing[19]. Comparing the three microstructures in Fig.8, it is found that with increasing Al content addition, the average grain size becomes smaller, and the average roundness decreases firstly and then increases (see Fig.9). When Al content is 2%, 4%, and 6%, the grain size is 65.3, 56.5, and 52.2 μm, and the roundness is 1.3, 1.19, and 1.23 respectively. Wang et al[20] studied the grain refinement mechanism of Al and Zn content on magnesium alloy from the point of the crystalline free phases, and established a classical mathematical model which can be used to assess the alloy microstructure.

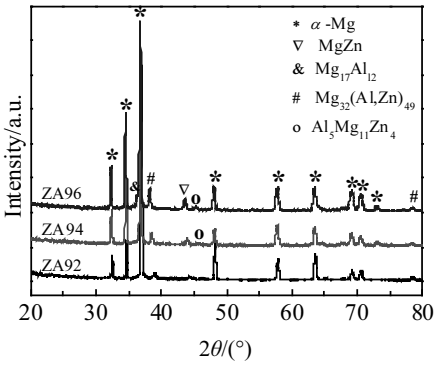

Fig.7 XRD patterns of Mg-9Zn-*X*Al alloy

Fig.10 shows the mechanical properties of rheo-casting samples at different Al additions and temperatures. It can be seen that with an increase of Al content, the comprehensive strength increases and comprehensive deformation decreases slightly. This may be due to the grain refined alloy and the increasing amount of the second phase(MgZn, $Mg_{32}(Al,Zn)_{49}$, and $Mg_{17}Al_{12}$), which hinders dislocation slip. At room temperature, the comprehensive strength of ZA92, ZA94, and ZA96 magnesium alloy are 358, 389, and 410MPa, and the comprehensive deformations are 13.13%, 13.8%, and 14.32% respectively. When the working temperature of the samples is between 20~150 °C，the comprehensive strength decreases slightly with an increase in operating temperature. However, the comprehensive strength decreases quickly for the ZA96 magnesium ally during 100~150 °C. This is because $Mg_{17}Al_{12}$,

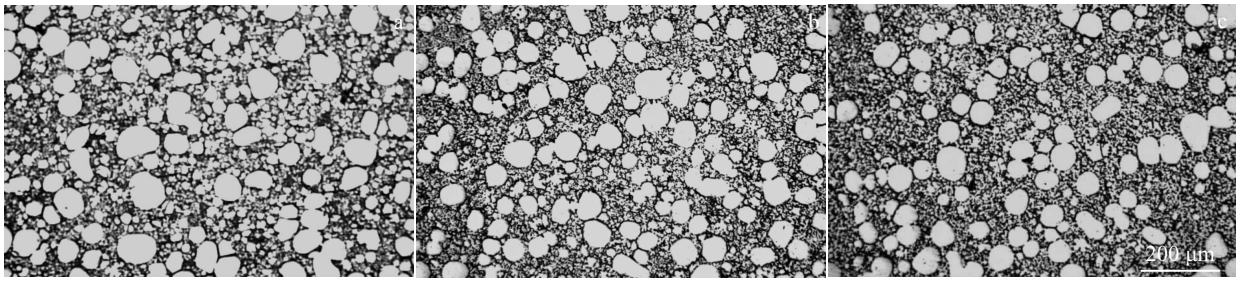

Fig.8 Rheo-casting microstructures of Mg-9Zn-*X*Al alloy: (a) ZA92, (b) ZA94, and (c) ZA96

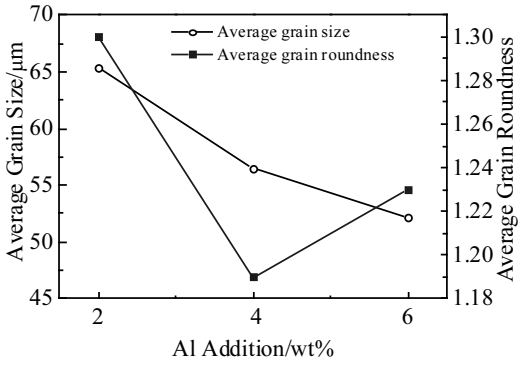

Fig.9 Average grain size and roundness of Mg-9Zn-*X*Al alloy

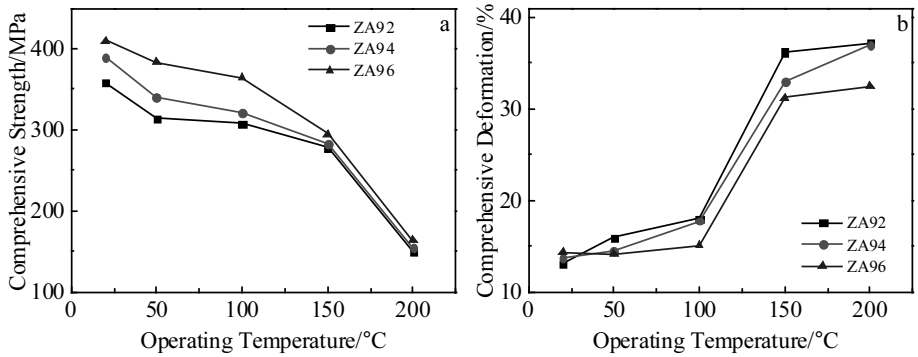

Fig.10 Comprehensive properties of Mg-9Zn-*X*Al alloy: (a) comprehensive strength and (b) comprehensive deformation

which only formed in ZA96, softens rapidly in this temperature range. The comprehensive deformation increases rapidly during 100~150 °C. When the working temperature is 150 °C, the comprehensive strengths of ZA92, ZA94 and ZA96 magnesium alloy are 278, 283, and 295 MPa, and the comprehensive deformation are 36.22%, 33.02%, and 31.21% respectively. When the operating temperature increases to 200 °C, the comprehensive strength decreases quickly, but the comprehensive deformation has no obvious change.

4 Conclusions

1) A larger temperature window is conducive to the control and operation of semi-solid forming for the Mg-9Zn-*X*Al (*X*=2, 4, 6) alloy, and the temperature sensitivity of all the solid fractions is smaller than 0.015.

2) Mg-9Zn-*X*Al alloy has different phase transformation temperatures and paths at different Al additions. α-Mg, MgZn, $Mg_{32}(Al, Zn)_{49}$, and $Al_5Mg_{11}Zn_4$ form in all samples. When Al addition increases to 6 wt%, the $Mg_{17}Al_{12}$ phase forms.

3) The grain size and roundness of Mg-9Zn-*X*Al alloys prepared by the self-inoculation rheo-diecasting method are 65.3, 56.5, 52.2 μm, and 1.3, 1.19, 1.23, respectively.

4) With the increase of Al content, the comprehensive strength increases, and the comprehensive deformation decreases slightly. Mg-9Zn-*X*Al alloys have better mechanical properties at a higher temperature. When the working temperature is 150 °C, the comprehensive strength and deformation are 278, 283, 295 MPa and 36.22%, 33.02%, 31.21%, respectively.

References

1 Hirsch J, Al-Samman T. *Acta Materilia*[J], 2013, 61(3): 818

2 Hu Y, Rao L, Li Q P *et al*. *Rare Metal Materials and Engineering*[J], 2016, 45(2): 493 (in Chinese)

3 Zhou B, Kang Y L, Qi M F *et al*. *Journal of Materials Engineering*[J], 2014, 42(10): 1 (in Chinese)

4 Wan X F, Ni H J, Huang M Y *et al*. *Transactions of Nonferrous Metals Society of China*[J], 2013, 23(4): 896

5 Chen Y A, Gao J J, Yu S *et al*. *Materials Science & Engineering A*[J], 2016, 671: 127

6 Feng K, Huang X F, Ma Y *et al*. *The Chinese Journal Nonferrous Metals*[J], 2011, 21(9): 2035 (in Chinese)

7 Mile B Djurdjecvic, Rainer Schmid-Fetzer. *Materials Science and Engineering A*[J], 2006, 417(1-2): 24

8 Agnew S R, Nie J F. *Scripta Materialia*[J], 2010, 63(7): 671

9 Maciel C A, Atkinson H V, Kapranos P. *Acta Materialia* [J], 2003, 51(8): 2319

10 Liu D, Atkinson H V, Jones H. *Acta Materialia*[J], 2005, 53(14): 3807

11 Li Y D, Apelian D, Xing B *et al*. *Transactions of Nonferrous Metals Society of China*[J], 2010, 20(9): 1572

12 GrÖbner J, Kozlov A, Fang X F *et al*. *Acta Materialia*[J], 2015, 90: 400

13 Liu J T, Zhang Y A, Li X W *et al*. *Transactions of Nonferrous Metals Society of China*[J], 2014, 24(5): 1481

14 Xia X Y, Sanaty-Zadeh A, Zhang C *et al*. *Journal of Alloys and Compounds*[J], 2014, 593: 71

15 Chen S L, Daniel S, Zhang F *et al*. *Calphad*[J], 2002, 26(2): 175

16 Pola A, Roberti R, Bertoli E *et al*. *Proceedings of the 9th S2P Advanced Semi-Solid Processing of Alloys and Composities*[C]. Busan: Trans Tech Publications LTD, 2006: 58

17 Gottardi G, Pola A, La Vecchia G M. *La Metallurgia Italiana*[J], 2015(5): 11

18 Anynwu L A, Kamado S, Honda T. *Materials Science Forum*[J], 2000, 350-351: 73

19 Xing B, Li Y D, Feng J Y *et al*. *Metals*[J], 2016, 6(3): 69

20 Wang C J, Jin Q L, Zhou R *et al*. *Rare Metal Materials and Engineering*[J], 2010, 39(S1): 208 (in Chinese)

Mg-9Zn-*X*Al 合金半固态成形的热力学分析及实验研究

李　春[1,2]，崔　乐[1]，范新会[1,2]，陈　建[1,2]，李　英[1]，袁训锋[1]，李元东[3]

(1. 商洛学院 陕西省尾矿综合利用重点实验室，陕西 商洛 726000)

(2. 西安工业大学，陕西 西安 710021)

(3. 兰州理工大学 省部共建有色金属先进加工与再利用国家重点实验室，甘肃 兰州 730050)

摘　要：采用相图计算软件 Pandat 计算了 Mg-9Zn-*X*Al(*X*=2, 4, 6，质量分数，%)合金的凝固温度窗口、固相率对温度的敏感性、加工温度窗口和相组成及其转变路径，并进行了实验验证。结果表明：Mg-9Zn-*X*Al 镁合金的半固态加工温度窗口较大，易于进行半固态成形操作，且在半固态加工温度区间，其固相率对温度的敏感性均小于 0.015。当 Al 含量不同时，其相的转变温度和路径不同。Mg-9Zn-*X*Al 在凝固过程中均形成 α-Mg、MgZn，$Mg_{32}(Al, Zn)_{49}$ 和 $Al_5Mg_{11}Zn_4$ 相，当 Al 含量增加至 6%时，形成了 $Mg_{17}Al_{12}$ 相。自孕育流变成形 Mg-9Zn-*X*Al 合金的晶粒尺寸和圆整度分别为 65.3、56.5、52.2 μm 和 1.3、1.19、1.23。当加工温度为 150 ℃时，其抗压强度和压缩变形量分别为 278、283、295 MPa 和 36.22%、33.02%、31.21%。

关键词：热力学分析；Mg-9Zn-*X*Al 合金；半固态成形；相转变

作者简介：李　春，男，1986 年生，博士生，讲师，商洛学院化学工程与现代材料学院，陕西 商洛 726000，E-mail: lic_slxy@163.com